remote sensing

MDPI

Article

A Novel Gridless Non-Uniform Linear Array Direction of Arrival Estimation Approach Based on the Improved Alternating Descent Conditional Gradient Algorithm for Automotive Radar System

Mingxiao Shao [1,2,3,*], Yizhe Fan [1,2,3], Yan Zhang [1,2,3], Zhe Zhang [2,3,4,5], Jie Zhao [6] and Bingchen Zhang [1,2,3]

[1] The Key Laboratory of Technology in Geo-Spatial Information Processing and Application System, Chinese Academy of Sciences, Beijing 100094, China
[2] The Aerospace Information Research Institute, Chinese Academy of Sciences, Beijing 100094, China
[3] School of Electronic, Electrical and Communication Engineering, University of Chinese Academy of Sciences, Beijing 101408, China
[4] The Suzhou Aerospace Information Research Institute, Suzhou 215123, China
[5] The National Key Laboratory of Microwave Imaging Technology, Beijing 100190, China
[6] Beijing Autoroad Technology Co., Ltd., Beijing 100102, China
* Correspondence: shaomingxiao20@mails.ucas.ac.cn

Abstract: In automotive millimeter-wave (MMW) radar systems, achieving high-precision direction of arrival (DOA) estimation with a limited number of array elements is a crucial research focus. Compressive sensing (CS) techniques have been demonstrated to offer superior performance in DOA estimation compared to spectral estimation methods. However, traditional CS methods suffer from an off-grid effect, which causes their reconstruction results to deviate from the actual positions of the signal sources, thereby reducing the accuracy. Currently, as a gridless method, atomic norm minimization (ANM) has shown effectiveness in DOA estimation for uniform linear arrays (ULAs). However, the performance of ANM is suboptimal in non-uniform linear arrays (NULAs), and their computational efficiency is not satisfactory. In this paper, we propose a novel algorithm for DOA estimation in NULA, drawing inspiration from the alternating descent conditional gradient algorithm framework. First, we construct an atomic set based on the observation scene and select the atoms with the highest correlation to the residuals as potential signal sources for global estimation. Then, we construct a mapping function for the signal sources in the continuous domain and perform conditional gradient descent in the neighborhood of each signal source, addressing the bias introduced by the off-grid effect. We compared the proposed algorithm with ANM, Iterative Shrinkage Thresholding (IST), and Multiple Signal Classification (MUSIC) algorithms. Simulation experiments validate that the proposed algorithm effectively addresses the off-grid effect and is applicable to DOA estimation in coprime and random arrays. Furthermore, real data experiments confirm the effectiveness of the proposed algorithm.

Keywords: compressive sensing; DOA estimation; off-grid effect; non-uniform linear array; millimeter-wave radar

check for updates

Academic Editor: Andrzej Stateczny

Received: 8 November 2024
Revised: 29 December 2024
Accepted: 13 January 2025
Published: 16 January 2025

Citation: Shao, M.; Fan, Y.; Zhang, Y.; Zhang, Z.; Zhao, J.; Zhang, B. A Novel Gridless Non-Uniform Linear Array Direction of Arrival Estimation Approach Based on the Improved Alternating Descent Conditional Gradient Algorithm for Automotive Radar System. *Remote Sens.* **2025**, *17*, 303. https://doi.org/10.3390/rs17020303

Copyright: © 2025 by the authors. Licensee MDPI, Basel, Switzerland. This article is an open access article distributed under the terms and conditions of the Creative Commons Attribution (CC BY) license (https://creativecommons.org/licenses/by/4.0/).

1. Introduction

Array signal processing remains one of the most popular research topics in the field of signal processing. Currently, direction of arrival (DOA) estimation has been widely applied in various domains such as autonomous driving, radar detection and channel

estimation, achieving satisfactory results [1–4]. It is important to note that in vehicular radar DOA estimation, the space available for array placement is limited, and the power supply of the vehicle is also constrained [5,6]. As a result, uniform linear arrays (ULAs) are not the optimal choice, whereas non-uniform linear arrays (NULAs) can offer significant advantages [7]. Additionally, in order to rapidly acquire information about the surrounding road environment, the accuracy and efficiency of DOA estimation are also critical factors that cannot be overlooked [8].

Initially, spectral estimation techniques, such as the multiple signal classification (MUSIC) [9–11] and estimation of signal parameters via rotational invariance techniques (ESPRIT) [12,13], were employed for DOA estimation. These algorithms construct a covariance matrix from the echo signals and estimate the angles by evaluating the eigenvalues of the covariance matrix. However, the performance of these algorithms is significantly affected when the number of snapshots is insufficient. Subsequently, compressive sensing (CS) techniques proposed by Candes and others have been widely recognized for their superior reconstruction accuracy and resolution capabilities compared to spectral estimation techniques [14,15]. CS-based DOA estimation algorithms can estimate the angles of signal sources using only a single snapshot of observation data and exhibit higher robustness [16].

Currently, CS techniques have been widely applied in DOA estimation. Tan et al. [17] applied CS techniques to coprime array DOA estimation and demonstrated through simulations that the CS algorithm outperforms the MUSIC algorithm. Li et al. [18] applied a sparse reconstruction method based on L1-norm to multi-shot DOA estimation for the ULA, achieving a super-resolution reconstruction of 1.5° with 24 array elements. Leite et al. [19] proposed a list-based maximum likelihood orthogonal matching pursuit algorithm for DOA estimation with NULA, verifying its effectiveness through experiments. Additionally, many scholars have conducted extensive research on the application of CS in DOA estimation [20–22].

Despite the remarkable achievements of CS in DOA estimation, it is important to note that traditional CS methods require the observation scene to be discretized into a series of grids and assume that the signal sources are located at these grid points when constructing the observation matrix. This assumption leads to the deviation of the estimated results from the actual positions of the signal sources, which is known as the off-grid effect [23–25]. The bias caused by the off-grid effect inevitably reduces the accuracy of the reconstruction results of traditional CS methods. Due to the restriction of the Restricted Isometry Property (RIP) condition [26,27], traditional CS methods cannot effectively solve the off-grid effect by infinitely refining the grid width.

Currently, the mainstream solution to the off-grid effect is gridless reconstruction methods based on atomic norm minimization (ANM) theory [28,29]. These methods solve a semidefinite programming (SDP) problem aimed at constructing the lowest rank Toeplitz matrix and then recover the frequencies composing the signal through Vandermonde decomposition of the Toeplitz matrix [30–32]. The ANM has been proven to perform well in ULA [33,34]. However, the ANM has significant drawbacks. Since the ANM algorithm requires the Vandermonde structure of the signal during the solution process, it cannot be directly applied to DOA estimation for NULAs. In many DOA estimation applications, it is difficult to ensure that the array is uniformly distributed, limiting the application of the ANM algorithm, such as in sparse array DOA estimation. Although some algorithms have been developed for NULAs, they require interpolating NULAs into ULAs [35]. Different interpolation methods lead to discrepancies between the fitted data and the corresponding ULA data, ultimately affecting the reconstruction results. Additionally, the computational complexity of ANM is approximately $\mathcal{O}(N^3.5)$, which results in low efficiency and poses significant challenges for its application in vehicular radar systems [36].

In addition to the ANM algorithm, many researchers have conducted studies to address the off-grid effect in DOA estimation. One approach treats the bias caused by grid discretization as an error and eliminates it through methods such as compensation or Bayesian estimation [37–39]. Another approach leverages the Hermitian Toeplitz structure of the data covariance matrix to decompose the matrix and extract parameters such as the angles of the signal sources [40–42].

Recently, Nicolas Boyd et al. [43] proposed the alternating descent conditional gradient (ADCG) method framework to rapidly address the off-grid effect, which has been applied in fields such as communication [44] and microscopy imaging [45]. The ADCG algorithm alternates between global conditional gradient descent and non-convex local search. The non-convex local search addresses the bias caused by the off-grid effect by performing conditional gradient descent within the neighborhood of the signal source using the mapping function of the signal source.

In this paper, we draw on the core ideas of the ADCG algorithm to propose a new algorithm suitable for DOA estimation with NULAs. The ADCG algorithm, during global conditional gradient descent, may fall into local optima, causing it to overlook the global optimum. To enhance the stability of the algorithm, we combine the strengths of traditional CS methods and the ADCG algorithm. In the global estimation, we discretize the observation scene to construct an atomic set. We estimate the angles of the signal sources by calculating the inner product of the atomic set with the residuals from each iteration, using these estimates as initial values for the local search. Subsequently, we construct a mapping function of the signal sources and perform conditional gradient descent within the neighborhood of each signal source for iterative optimization. This step is computed in the continuous domain, effectively addressing the off-grid effect. We name our proposed algorithm the CS-ADCG algorithm.

The structure of this paper is as follows. In Section 2, we construct the mathematical model for DOA estimation with arbitrary array forms and the ADCG framework. In Section 3, we introduce the proposed CS-ADCG algorithm and apply it to DOA estimation with arbitrary array forms. In Section 4, we simulate DOA estimation for an automotive millimeter-wave (MMW) radar system, design simulation experiments, compare the proposed algorithm with the ANM [30,35], IST [46], and MUSIC [9] algorithms, and analyze the resolution capability and robustness of the proposed algorithm for ULA and NULA. In Section 5, we use an automotive MMW radar to collect three sets of real data, comparing the performance of the four algorithms in real data processing. Finally, Section 6 concludes the article.

2. Automotive MMW Radar Signal Model and the ADCG Algorithm

2.1. Automotive MMW Radar Signal Model

Compared to ULA, NULA has several advantages, such as coprime arrays and nested arrays. Most of the array element spacings in these arrays are longer than half a wavelength, which reduces mutual coupling effects between elements. The sparse placement of elements extends the array aperture, thereby achieving higher accuracy and resolution in DOA estimation. Assume an array with N elements. For generality, we assume the first element is located at the origin on the coordinate axis, and the remaining $N-1$ elements are positioned at coordinates given by the d_n where $n = 2, 3, \cdots, N$. The array elements can thus be represented by the vector $\boldsymbol{d} = [d_1, d_2, \cdots, d_N]$. Assuming K narrowband signals are irradiated onto the array from $\theta = [\theta_1, \theta_2, \cdots, \theta_K]$, where θ_k ($k = 1, 2, \cdots, K$) is defined as the angle of the k-th source. Assuming that the source is far enough from the array, the received signal can be considered as a plane wave. We only consider the case of a single measurement snapshot, where the steering vector of the array is

$$\boldsymbol{a}(\theta_k) = [1, \exp(-j\omega_2(\theta_k)), \cdots, \exp(-j\omega_N(\theta_k))]^T, \tag{1}$$

where $(\bullet)^{\mathrm{T}}$ represents transpose operation and

$$\omega_n(\theta_k) = 2\pi(n-1)\frac{d_n}{\lambda}\sin(\theta_k), n = 1, 2, \cdots, N. \tag{2}$$

The steering matrix can be constructed based on the steering vector

$$\boldsymbol{A} = [\boldsymbol{a}(\theta_1), \boldsymbol{a}(\theta_2), \cdots, \boldsymbol{a}(\theta_K)] \in \mathbb{C}^{N\times K}. \tag{3}$$

The response of K narrowband signals received by the array is

$$\begin{aligned} \boldsymbol{y} &= \sum_{k=1}^{K} \boldsymbol{a}(\theta_k)s_k + \boldsymbol{n} \\ &= \boldsymbol{A}\boldsymbol{s} + \boldsymbol{n}, \end{aligned} \tag{4}$$

where $\boldsymbol{y} \in \mathbb{C}^{N\times 1}$, $\boldsymbol{s} = [s_1, s_2, \cdots, s_K]^T$ is the scattering coefficient of the signal sources, $\boldsymbol{n} \in \mathbb{C}^{N\times 1}$ is gaussian white noise.

Considering the sparsity of signal sources in space, the angle of the signal source can be estimated by CS methods. We discretize the observation angle range into a set of grids. When there is a signal source in a grid, the value of the grid is the scattering coefficient of the signal source; otherwise, it is 0. The grids in the observation scene are arranged as a vector $\boldsymbol{x} \in \mathbb{C}^{M\times 1}$ where M is the number of grids. The automotive MMW radar DOA estimation model based on CS can be expressed as

$$\boldsymbol{y} = \boldsymbol{\Phi}\boldsymbol{x} + \boldsymbol{n}, \tag{5}$$

where $\boldsymbol{\Phi} \in \mathbb{C}^{N\times M}$ is the observation matrix.

The objective of DOA estimation of automotive MMW radar is to estimate the non-zero values in $\boldsymbol{x}$ from the received signal $\boldsymbol{y}$. Since each element in $\boldsymbol{x}$ corresponds to a discrete angle, the non-zero positions in $\boldsymbol{x}$ uniquely determine the angles of the signal sources.

2.2. The ADCG Algorithm for Gridless Sparse Reconstruction

The ADCG algorithm formalizes a general approach for solving sparse inverse problems, building upon the classic conditional gradient method (CGM) [43,47]. The ADCG algorithm combines the rapid local convergence properties of nonlinear programming algorithms with the stability and global convergence guarantees associated with convex optimization.

We assume that each signal source possesses a non-negative weight $w > 0$. The parameters describing the signal sources are denoted by γ, and $\gamma \in \Gamma$, where Γ is continuously distributed in practical applications. Assuming there are K signal sources in the space, the observed signal can be described as

$$\boldsymbol{b} = \sum_{k=1}^{K} w^{(k)}\boldsymbol{\psi}(\gamma^{(k)}) \in \mathbb{C}^{N\times 1}, \tag{6}$$

where $\boldsymbol{b}$ is the observed signal, $w^{(k)}$ is the weight of the k-th signal source, $\boldsymbol{\psi} : \Gamma \to \mathbb{C}^{N\times 1}$ is the mapping function. It is important to note that the successful execution of the ADCG algorithm is predicated on the condition that the mapping function $\boldsymbol{\psi}$ is differentiable.

We discretize the parameter space Γ of the signal sources into an atomic measure μ with mass $w^{(k)}$ at $\gamma^{(k)}$. The signal sources are represented as

$$\boldsymbol{\mu} = \sum_{k=1}^{K} w^{(k)} \delta_{\gamma^{(k)}}. \tag{7}$$

We define the observation process as an observation matrix $\boldsymbol{\Omega}$ based on an overcomplete set of atoms. The reconstruction of source parameters can be achieved by minimizing the convex loss function of the residual between the noisy observed signal $\boldsymbol{b}$ and $\boldsymbol{\Omega\mu}$.

$$\begin{aligned} &\min \ell(\boldsymbol{\Omega\mu} - \boldsymbol{b}) \\ &\text{s.t. } \boldsymbol{\mu} \geq 0, \\ &\quad \boldsymbol{\mu}(\Gamma) < \epsilon. \end{aligned} \tag{8}$$

Here, $\ell(\cdot)$ is the convex loss function, and $\epsilon > 0$ is a parameter that controls the total mass of $\boldsymbol{\mu}$ and empirically controls the cardinality of solutions to (8).

The ADCG algorithm estimates the parameters of signal sources in each iteration through a global rough estimation and a local update.

The objective of the global rough estimation is to identify an atom that approximates the true source closely. This step, akin to the classic CGM, is accomplished by minimizing the linearized objective in the parameter space for the k-th iteration

$$\gamma^{(k)} k \in \underset{\gamma \in \Gamma}{\operatorname{argmin}} \left\langle \boldsymbol{\psi}(\gamma), g^{(k)} \right\rangle, \tag{9}$$

where g_k represents the gradient of the convex loss function and $\langle \cdot, \cdot \rangle$ is defined as the inner product operator.

$$g^{(k)} \leftarrow \nabla \ell(\boldsymbol{\Omega\mu}^{(k-1)} - \boldsymbol{b}). \tag{10}$$

As a result of rough estimation, $\gamma^{(k)}$ is included in a support set $\boldsymbol{S}^{(k)}$.

$$\boldsymbol{S}^{(k)} \leftarrow \boldsymbol{S}^{(k-1)} \cup \gamma^{(k)}, \tag{11}$$

where the symbol "$\cup$" represents the union operation.

The purpose of the local update is to estimate the parameters of the signal sources more accurately based on the results of the rough estimation. Initially, the weights of the signal sources are estimated based on the rough estimates within the support set.

$$w^{(k)} \leftarrow \underset{\boldsymbol{\mu} \geq 0, \boldsymbol{\mu}(S^{(k)}) < \epsilon}{\operatorname{argmin}} \ell\Big(\sum_{\gamma \in S^{(k)}} \boldsymbol{\mu}(\gamma) \boldsymbol{\psi}(\gamma) - \boldsymbol{b} \Big). \tag{12}$$

Subsequently, the support set is pruned based on the weights. The classic CGM introduces a new atom with each iteration, leading to a non-sparse reconstruction of the signal due to incorrectly introduced atoms as the number of iterations increases. To maintain the sparsity of the signal, ADCG eliminates incorrect outcomes from the current support set in each iteration, thus preserving the sparsity of the estimated signal.

$$S^{(k)} = \operatorname{support}(w^{(k)}). \tag{13}$$

Finally, with the number of sources already determined, local updates on the parameters within the pruned support set are more accurately estimated over a continuous domain. This local update can be realized through a non-convex optimization.

$$\begin{aligned} \min\ & \ell\left(\sum_{i=1}^{k} w^{(i)} \boldsymbol{\psi}(\gamma^{(i)}) - \boldsymbol{b}\right) \\ & \gamma^{(i)} \in \Gamma, \\ \text{s.t. } & w^{(i)} > 0, \\ & \sum_{i} w^{(i)} < \epsilon. \end{aligned} \tag{14}$$

The overall steps of the ADCG algorithm are listed in Algorithm 1. It should be noted that **local_descent** in Algorithm 1 is a subroutine that can be solved using (14).

Algorithm 1 Alternating descent conditional gradient method (ADCG).

Input: K, $\boldsymbol{b}$, $\boldsymbol{\Omega}$, $S^{(0)} = \varnothing$
For $k = 1 : K$
1: Compute gradient of loss: $g^{(k)} \leftarrow \nabla \ell(\boldsymbol{\Omega}\boldsymbol{\mu}^{(k-1)} - \boldsymbol{b})$
2: Compute next source: $\gamma^{(k)} \in \underset{\gamma \in \Gamma}{\operatorname{argmin}} \left\langle \boldsymbol{\psi}(\gamma), g^{(k)} \right\rangle$
3: Update support: $S^{(k)} \leftarrow S^{(k-1)} \cup \gamma^{(k)}$
4: Coordinate descent on nonconves objective:
5: **Repeat** :
6: Compute weights:
$w^{(k)} \leftarrow \underset{\boldsymbol{\mu} \geq 0, \boldsymbol{\mu}(S^{(k)}) < \epsilon}{\operatorname{argmin}} \ell\left(\sum_{\gamma \in S^{(k)}} \boldsymbol{\mu}(\gamma)\boldsymbol{\psi}(\gamma) - \boldsymbol{b}\right)$
7: Prune support: $S^{(k)} = \operatorname{support}(w^{(k)})$
8: Locally improve support:
$S^{(k)} = \textbf{local_descent}((\gamma, \boldsymbol{\mu}^{(k)}(\gamma)) : \gamma \in S^{(k)})$
Output: $\{(\gamma^{(1)}, w^{(1)}), \ldots, (\gamma^{(K)}, w^{(K)})\}$

3. CS-ADCG Algorithm for Gridless Automotive MMW Radar DOA Estimation

Although many sparse reconstruction algorithms currently exist for estimating (5), traditional CS methods are subject to the off-grid effect. In DOA estimation, as the grid width becomes denser, the dimension of the observation matrix increases drastically, making algorithm implementation more challenging. To address this issue, we have improved the rough estimation approach of the classic ADCG algorithm and propose the CS-ADCG algorithm. Although traditional CS algorithms are affected by the off-grid effect, they can typically reconstruct the parameters of signal sources effectively. Inspired by traditional CS algorithms, we discretize the azimuthal observation angle into a set of rough grids. Utilizing traditional CS algorithms, we roughly estimate the angles of the signal sources and use these estimates as initial values for local updates.

The CS-ADCG algorithm minimizes the loss function $\ell(\boldsymbol{\theta})$, which represents the residual between the observed signal $\boldsymbol{y}$ and the reconstructed signal $\boldsymbol{\Phi x}$, aiming to estimate the true values of the signal.

$$\begin{aligned} & \min \ell(\boldsymbol{\Phi x} - \boldsymbol{y}) \\ & \text{s.t. } \boldsymbol{x} \geq 0 \\ & \quad \boldsymbol{x}(\boldsymbol{\theta}) < \epsilon. \end{aligned} \tag{15}$$

For the k-th source, we define its parameters as $\{\theta_{\mathcal{A}}^{(k)}, \theta_{\mathcal{W}}^{(k)}\}$, where $\theta_{\mathcal{A}}^{(k)}$ is angle, and $\theta_{\mathcal{W}}^{(k)}$ is the scattering coefficient. We divide the angles into a set of rough grids, based on which we construct an atom set denoted as $\boldsymbol{\Phi} = \{\boldsymbol{\phi}_1, \boldsymbol{\phi}_2, \cdots, \boldsymbol{\phi}_M\}$. The grids for discretized

angles do not need to be dense, in order to reduce computational costs. In the process of selecting potential sources, we first calculate the correlation between the atom set and the residual vector $\boldsymbol{r}(\boldsymbol{\theta})$. Then, we choose the atom group with the highest correlation as the result of the rough estimation. This process can be expressed as

$$\theta_{\mathcal{A}}^{(k)} \leftarrow \text{argmax}\langle \boldsymbol{\phi}_j, \boldsymbol{r}^{(k)}(\boldsymbol{\theta})\rangle, \phi_j \in \boldsymbol{\Phi}. \tag{16}$$

The selected $\theta_{\mathcal{A}}^{(k)}$ is added to the support set

$$\boldsymbol{S}^{(k)} = \{\boldsymbol{\theta}_{\mathcal{A}}^{(k)}, \boldsymbol{\theta}_{\mathcal{W}}^{(k-1)}\}, \tag{17}$$

where

$$\boldsymbol{\theta}_{\mathcal{A}}^{(k)} = [\theta_{\mathcal{A}}^{(1)}, \theta_{\mathcal{A}}^{(2)}, \cdots, \theta_{\mathcal{A}}^{(k)}], \tag{18}$$

$$\boldsymbol{\theta}_{\mathcal{W}}^{(k-1)} = [\theta_{\mathcal{W}}^{(1)}, \theta_{\mathcal{W}}^{(2)}, \cdots, \theta_{\mathcal{W}}^{(k-1)}]. \tag{19}$$

$\theta_{\mathcal{A}}^{(k)}$ is the angle estimated in the k-th iteration. The bolded $\boldsymbol{\theta}_{\mathcal{A}}^{(k)}$ is the set of k angles $\theta_{\mathcal{A}}^{(k)}$ after k iterations. Similarly, $\theta_{\mathcal{W}}^{(k-1)}$ is the scattering coefficient estimated in the $(k-1)$-th iteration. The bolded $\boldsymbol{\theta}_{\mathcal{W}}^{(k-1)}$ is the set of $(k-1)$ scattering coefficients $\theta_{\mathcal{W}}^{(k-1)}$ after $(k-1)$ iterations.

We estimate the scattering coefficients of atoms in the support set $\boldsymbol{S}^{(k)}$. Once the atom group is determined, the scattering coefficients can be effectively obtained by solving the least-squares problem

$$\theta_{\mathcal{W}}^{(k)} = \frac{\tilde{\boldsymbol{\phi}}^H}{\tilde{\boldsymbol{\phi}}^H \tilde{\boldsymbol{\phi}}} \boldsymbol{y}, \tag{20}$$

where $\tilde{\boldsymbol{\phi}}^H$ represents the chosen atom group set, and $(\bullet)^H$ denotes the conjugate transpose. Based on the results of rough estimation, the loss function is updated by

$$\boldsymbol{r}(\boldsymbol{\theta}_{\mathcal{A}}^{(k)}, \boldsymbol{\theta}_{\mathcal{W}}^{(k)}) = \boldsymbol{y} - \sum_{i=1}^{k} \theta_{\mathcal{W}}^{(i)} \exp(-j\boldsymbol{\omega}(\theta_{\mathcal{A}}^{(i)})^T). \tag{21}$$

According to (1) and (2), the mapping functions are given by

$$\psi(\theta) = \exp(-j2\pi(n-1)\frac{d_n}{\lambda}\sin(\theta)), n = 1, 2, \cdots, N. \tag{22}$$

For the local update, we use the ℓ_2 norm as the loss function. As the number of parameters in the support set is fixed, the local fine estimation can be formulated as a non-convex optimization problem.

$$\begin{aligned} &\min \left|\left| \textstyle\sum_{i=1}^{K} \theta_{\mathcal{W}}^{(i)} \exp(-j\boldsymbol{\omega}(\theta_{\mathcal{A}}^{(i)})) - \boldsymbol{y} \right|\right|_2^2 \\ &\quad \theta^{(i)} \in \boldsymbol{S}^{(k)}, \\ &\text{s.t. } \theta_{\mathcal{W}}^{(i)} > 0, \\ &\quad \sum_i \theta_{\mathcal{W}}^{(i)} < \epsilon, \end{aligned} \tag{23}$$

where

$$\boldsymbol{\omega}(\theta_{\mathcal{A}}^{(i)}) = [\omega_1(\theta_{\mathcal{A}}^{(i)}), \omega_2(\theta_{\mathcal{A}}^{(i)}), \cdots, \omega_N(\theta_{\mathcal{A}}^{(i)})]^T. \tag{24}$$

For the non-convex optimization problem in (22), we use the rough estimation results as initial values and perform gradient descent for the mapping functions to estimate the accurate angles.

The complete process of our proposed CS-ADCG algorithm is shown in Algorithm 2.

Algorithm 2 CS-ADCG.

Input: K, $\boldsymbol{y}$, $\boldsymbol{\Phi}$, $\boldsymbol{r}^{(0)} = \varnothing$, $\boldsymbol{S}^{(0)} = \varnothing$
For $k = 1 : K$

1: Compute next source:
$\theta_{\mathcal{A}}^{(k)} \leftarrow \text{argmax} \left\langle \boldsymbol{\phi}_j, \boldsymbol{r}^{(k)}(\boldsymbol{\theta}) \right\rangle, \boldsymbol{\phi}_j \in \boldsymbol{\Phi}.$
2: Update support: $\boldsymbol{S}^{(k)} \leftarrow \boldsymbol{S}^{(k-1)} \cup \theta_{\mathcal{A}}^{(k)}$
3: Compute weights: $\theta_{\mathcal{W}}^{(k)} = \dfrac{\boldsymbol{\phi}'^{H}}{\boldsymbol{\phi}'^{H}\boldsymbol{\phi}'}\boldsymbol{y}$
4: Update residual:
$\boldsymbol{r}^{(k)}(\boldsymbol{\theta}) = \boldsymbol{y} - \sum_{i=1}^{k} \theta_{\mathcal{W}}^{(i)} \exp(-j2\pi\xi\theta_{\mathcal{A}}^{(i)})$
5: Coordinate descent on non-conves objective:
6: Locally improve support:
$\theta_{\mathcal{A}}^{(K)} \leftarrow \text{argmin} \left|\left| \sum_{i=1}^{K} \theta_{\mathcal{W}}^{(i)} \psi(\theta_{\mathcal{A}}^{(K)}) - \boldsymbol{y} \right|\right|_2^2.$

Output: $\theta = \{(\theta_{\mathcal{A}}^{(1)}, \theta_{\mathcal{W}}^{(1)}), \ldots, (\theta_{\mathcal{A}}^{(K)}, \theta_{\mathcal{W}}^{(K)})\}$

4. Simulation Experiments

To analyze the performance of the proposed algorithm, we conducted simulation experiments comparing CS-ADCG with ANM, IST and MUSIC algorithms, evaluating the reconstruction quality of the DOA estimation results. In the simulations, we considered ULA, random linear array (RLA), and coprime linear array (CLA)—three types of array configurations. The ULA and RLA both consist of 20 elements. The CLA consists of two ULAs containing 7 and 5 elements, respectively. The element distributions of the three arrays are shown in Figure 1. In the experiments evaluating the impact of signal-to-noise ratio (SNR) and angular intervals on DOA estimation results, we set up scenarios with only two signal sources. Subsequently, we conducted experiments to assess the DOA estimation quality for different numbers of signal sources and array elements, respectively.

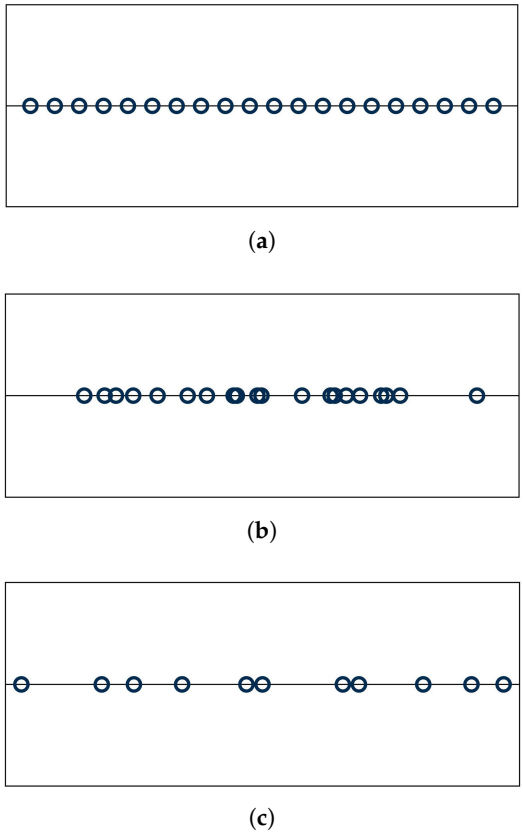
We used root mean square error (RMSE) and reconstruction success rate as evaluation metrics. RMSE is defined as

$$\text{RMSE} = \sqrt{\frac{1}{K}\sum_{i=1}^{K}(\theta_i - \hat{\theta}_i)^2}, \tag{25}$$

where θ_i represents the true angles, and $\hat{\theta}_i$ represents the estimated angles. For the reconstruction success rate, we consider the reconstruction to be successful when

$$\left|\theta_i - \hat{\theta}_i\right| \leq \theta_{th}, \tag{26}$$

where θ_{th} is the threshold for the success rate. Since ANM cannot be directly applied to DOA estimation for the RLA, we only compared the CS-ADCG with the IST and MUSIC algorithms in the RLA experiments. The simulation experiments were conducted on a laptop with a 3.20 GHz AMD R7-5800H CPU and 64 GB RAM.



(**a**)

(**b**)

(**c**)

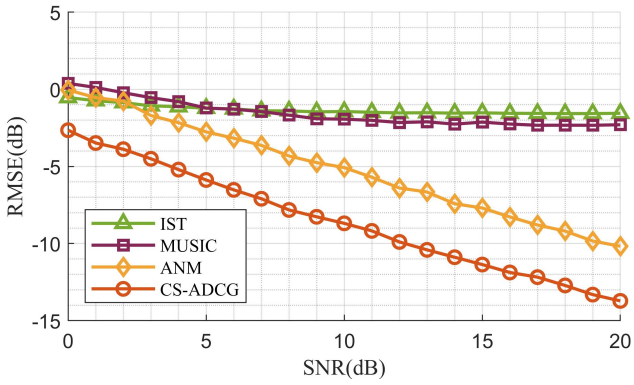
Figure 1. Schematic diagrams of the models for ULA, RLA and CLA used in the experiments. The circles in the figure represent the positions of the array elements. (**a**) The ULA. (**b**) The RLA. (**c**) The CLA.

4.1. Accuracy and Robustness Analysis

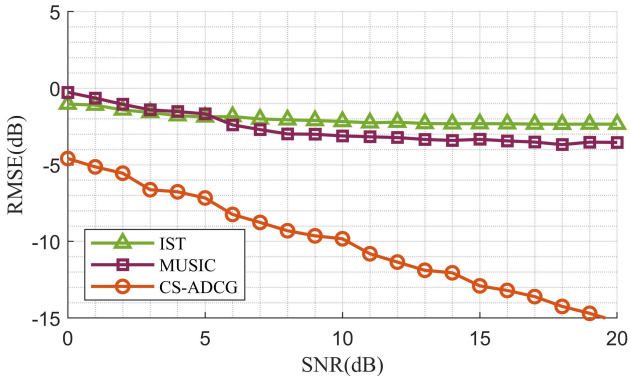
In this section, we analyze the reconstruction performance of the CS-ADCG algorithm compared to other algorithms under different SNRs. We randomly generate two signal sources within the angular range of -45° to 45°, with an angular separation of 2ρ between them, where ρ represents the rayleigh resolution of the ULA at 0°. The SNR is varied between 0 dB and 20 dB. It should be noted that when calculating the spatial spectrum across the angular range for the MUSIC algorithm, the angle step size is set to 0.1°. As a traditional CS algorithm, the IST algorithm requires the angular range to be divided into a set of grids to construct the observation matrix. Similarly, the grid width for the IST algorithm is set to 0.1°. The grid width for the CS-ADCG algorithm is set to 1° in the global estimation. Each experimental configuration is repeated 500 times, and the results are averaged.

For traditional CS algorithms, the reconstruction results can only lie on the pre-defined grids. Therefore, at high SNRs, the grid resolution is the primary factor limiting the reduction in the RMSE. Figure 2 shows the RMSE curves of four algorithms under different SNRs. During RMSE evaluation, we excluded obvious outliers. As shown in Figure 2, the RMSE curve of the IST algorithm does not converge with increasing SNR, constrained by the grid resolution in the angular domain. Similarly, the RMSE curve of the MUSIC algorithm, which searches for potential signal sources based on the pre-defined angle step size, exhibits a similar trend as the IST algorithm. In contrast, the RMSE curve of the CS-ADCG algorithm converges with increasing SNR, indicating that the estimation results of the CS-ADCG algorithm are not restricted by the grid, effectively addressing the off-grid effect. Furthermore, as shown in Figure 2b,c, the CS-ADCG algorithm is

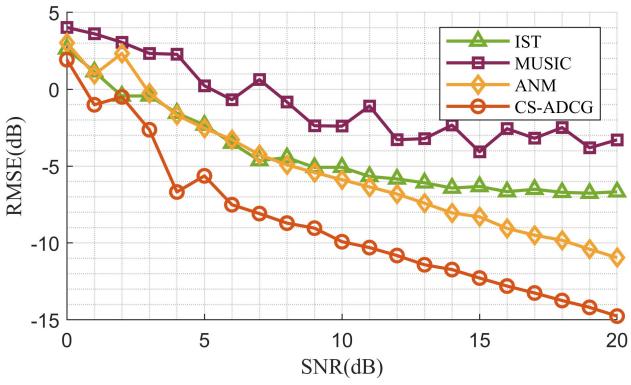
effective for both RLA and CLA, achieving superior reconstruction results compared to the comparative algorithms.



(**a**)



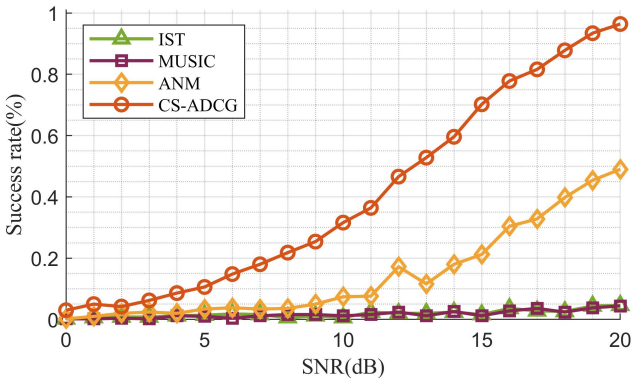
(**b**)



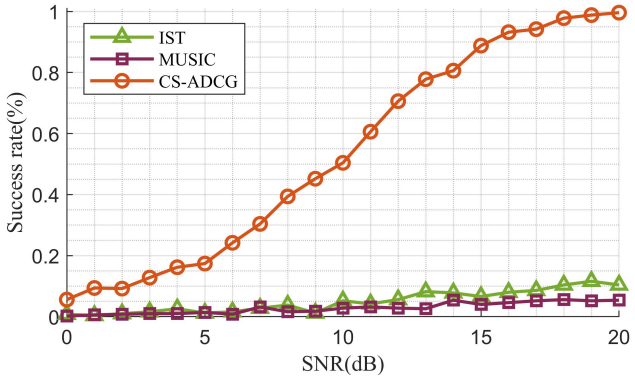
(**c**)

Figure 2. Comparison of the RMSE of CS-ADCG, ANM, IST, and MUSIC algorithms under different SNRs for the three types of arrays. (**a**) The ULA. (**b**) The RLA. (**c**) The CLA.

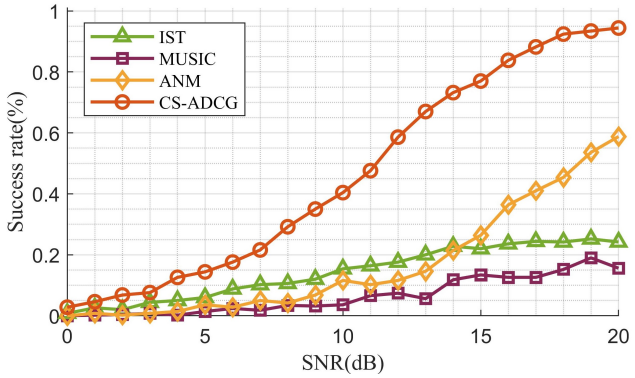
When evaluating the success rate, we set the threshold θ_{th} to 0.1°. Figure 3 shows the reconstruction success rate under different SNRs. From Figure 3, it is evident that as the SNR increases, the success rate of the CS-ADCG algorithm significantly surpasses that of the comparative algorithms. This demonstrates that compared to ANM, IST, and MUSIC algorithms, the CS-ADCG algorithm exhibits greater robustness.



(**a**)



(**b**)



(**c**)

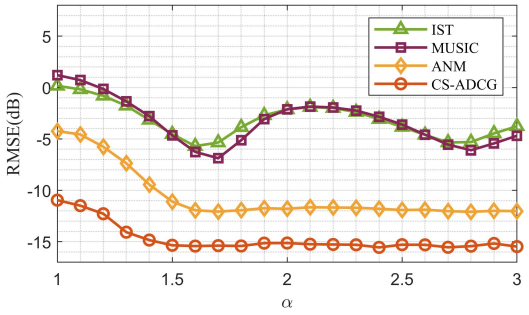
Figure 3. Comparison of the success rate of CS-ADCG, ANM, IST, and MUSIC algorithms under different SNRs for the three types of arrays. (**a**) The ULA. (**b**) The RLA. (**c**) The CLA.

4.2. Resolution Analysis

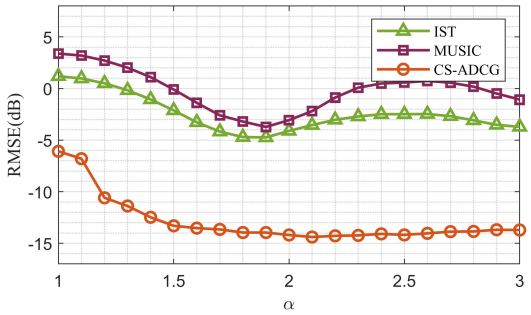
To analyze the resolution capability of the CS-ADCG algorithms, we compared the reconstruction performance of the four algorithms with two signal sources at different angular intervals. We randomly generate one signal source, while the azimuth angle of the second signal source is separated from the first by $\alpha\rho$, where α is the normalized distance and varies from 1 to 3 in steps of 0.1. The SNR is set to 20 dB. The same as in Section 4.1, we set the grids of the IST and MUSIC algorithm to 0.1°. The grid width for the CS-ADCG algorithm is set to 1° in the global estimation. When evaluating the success rate, we presented the curve at the success rate threshold $\theta_{th} = 0.1°$. Each experimental configuration is repeated 500 times, and the results are averaged. Figure 4 shows the RMSE of the DOA estimation of four algorithms at different angular intervals. Figure 5 shows the success rate of the DOA estimation for different angular intervals.

As shown in Figure 4, the CS-ADCG algorithm consistently maintains the lowest RMSE across the α range from 1 to 3, compared to the ANM, IST, and MUSIC algorithms. This indicates that the angles reconstructed by the CS-ADCG algorithm are closer to the true angles. Figure 5 reveals that although the success rates of the four algorithms fluctuate slightly with varying angular intervals, the success rate of the CS-ADCG algorithm is consistently higher than that of the ANM, IST, and MUSIC algorithms. This demonstrates that the CS-ADCG algorithm exhibits superior resolution performance compared to the three baseline algorithms, which is a significant improvement for automotive MMW radar systems.

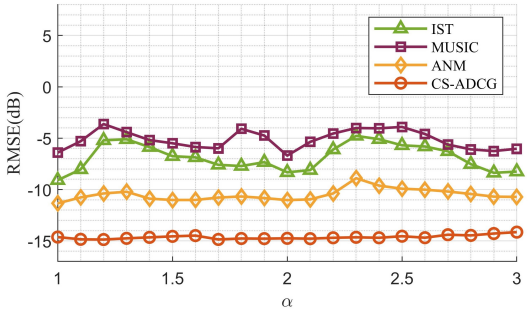
In the cases of ULA and RLA, as the angular interval increases, the reconstruction success rate of the CS-ADCG algorithm approaches 100%. This indicates that the CS-ADCG algorithm can stabilize the reconstruction result within 0.1° of the true value. In experiments with CLA, the success rates of the four algorithms exhibit some fluctuations. This is because, as a type of sparse array, the CLA uses fewer elements over a larger aperture, which is equivalent to downsampling the echo data of a ULA. The reduced amount of echo data decreases the stability of the algorithms. Nonetheless, the reconstruction success rate of the CS-ADCG algorithm remains above 90% in most cases.



(**a**)



(**b**)



(**c**)

Figure 4. Comparison of the RMSE of CS-ADCG, ANM, IST, and MUSIC algorithms under different angular intervals for the three types of arrays. (**a**) The ULA. (**b**) The RLA. (**c**) The CLA.

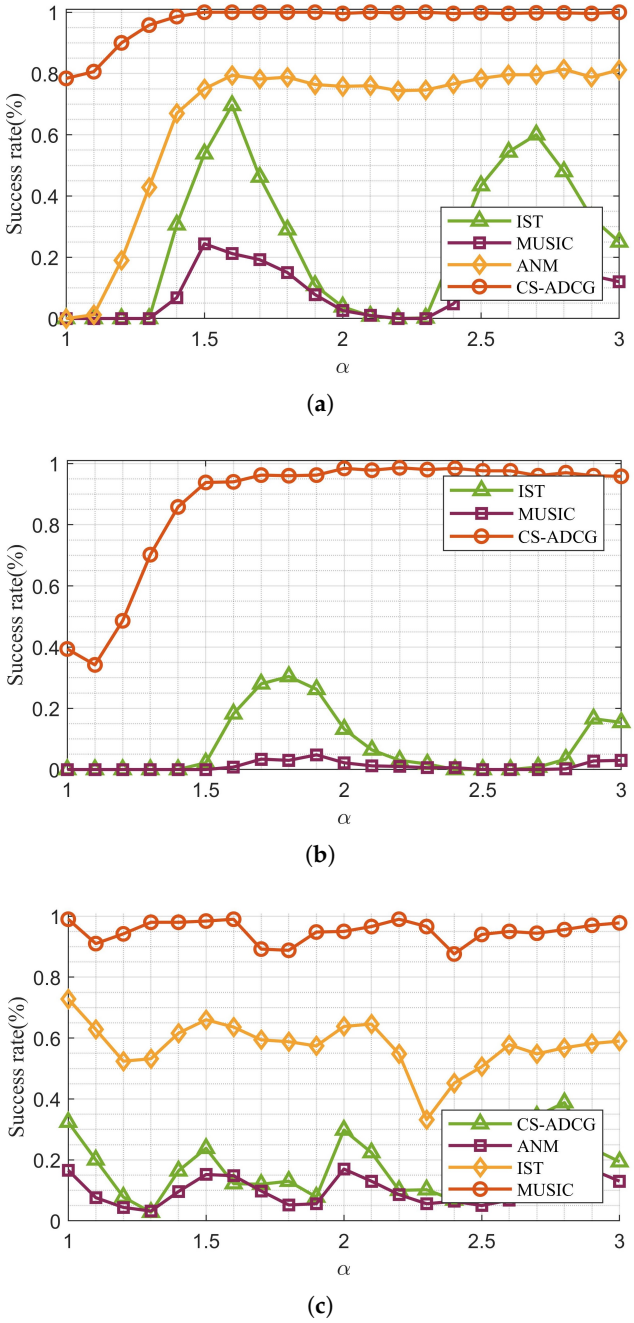


Figure 5. Comparison of the success rate of CS-ADCG, ANM, IST, and MUSIC algorithms under different angular intervals for the three types of arrays. (**a**) The ULA. (**b**) The RLA. (**c**) The CLA.

4.3. Comparison of Different Sparsities

To evaluate the DOA estimation performance under varying levels of sparsity, we randomly generate K ($K = 1, 2, \cdots, 4$) signal sources within the range of $[-45°, 45°]$. When $K > 1$, the spacing between the K sources is not less than 2ρ. The SNR is set to 20 dB. Each experiment is repeated 500 times, and the final results are averaged over these 500 trials. Figure 6 shows the RMSE of DOA estimation of four algorithms under different sparsities, while Figure 7 shows the reconstruction success rate of four algorithms under the same conditions. A reconstruction is considered successful if the estimated angle of the signal source differs from the true value by less than 0.1°.

From Figures 6 and 7, it can be observed that the performance of all four algorithms tends to degrade as the number of signal sources increases. Nevertheless, the CS-ADCG algorithm consistently outperforms the ANM, IST, and MUSIC algorithms. Under the

0.1° success rate threshold, the IST and MUSIC algorithms achieve a success rate higher than 80% only when $K = 1$. As sparsity increases, the performance of IST and MUSIC declines significantly. Similarly, the success rate of ANM also decreases with increased sparsity, though it remains superior to IST and MUSIC. The proposed CS-ADCG algorithm maintains a success rate above 80% in ULA and RLA experiments, with a slight drop below 80% only when $K = 4$ in the CLA experiment.

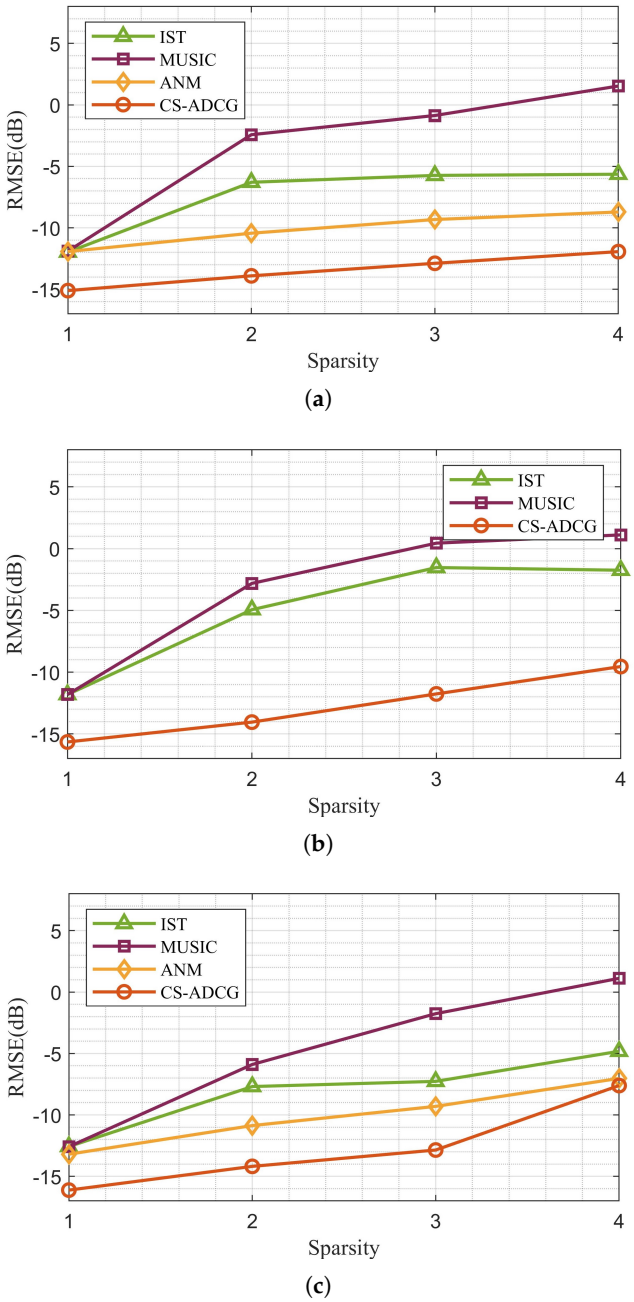
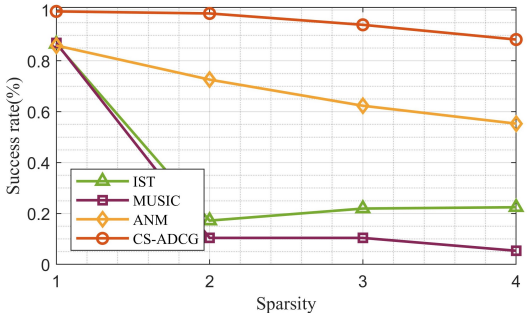
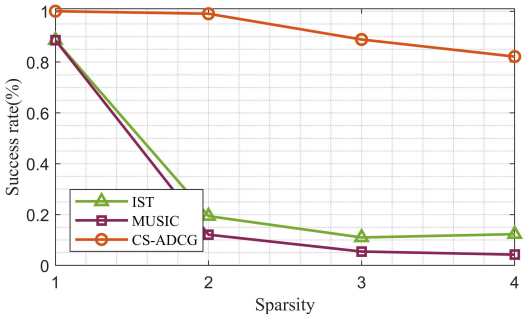


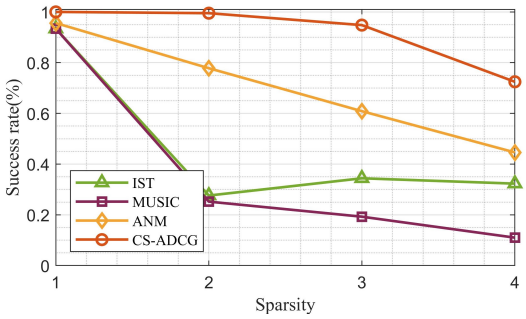
Figure 6. Comparison of the RMSE of CS-ADCG, ANM, IST, and MUSIC algorithms under different sparsities for the three types of arrays. (**a**) The ULA. (**b**) The RLA. (**c**) The CLA.



(**a**)



(**b**)



(**c**)

Figure 7. Comparison of the success rate of CS-ADCG, ANM, IST, and MUSIC algorithms under different sparsities for the three types of arrays. (**a**) The ULA. (**b**) The RLA. (**c**) The CLA.

4.4. Efficiency Comparison Under Different Numbers of Array Elements

The computational time of DOA estimation algorithms is crucial for automotive MMW radar systems. The computational time is closely related to the number of array elements. Therefore, we analyze the computational time of different algorithms when the number of array elements varies. To evaluate the time of DOA estimation, we set the number of elements for ULA and RLA to 20, 60, 100, 150 and 200, and the number of actual elements for CLA to 11, 17, 20, 25 and 30. We randomly generate 500 signal sources within the range of $[-45°, 45°]$, and record the total time taken by each algorithm to estimate the DOA of the 500 sources. The SNR is set to 20 dB. The final experimental results are the average of 10 trials. Table 1 presents the running times of the four algorithms.

As shown in Table 1, the running time of all four algorithms increases with the number of array elements. For the same number of elements, the running time of CS-ADCG is significantly shorter than that of ANM. In particular, for CLA, the running time of ANM becomes too long to be applicable in automotive MMW radar systems. In contrast, CS-ADCG reconstructs the 500 signal sources in less than 1 second, making it more feasible for automotive MMW radar systems compared to ANM.

Table 1. The running time of CS-ADCG, ANM, IST, and MUSIC algorithms under different numbers of elements for the three types of arrays. The unit of numerical value is seconds.

Number		20	60	100	150	200
ULA	CS-ADCG	0.70	0.76	1.01	1.58	1.95
	ANM	48.07	78.25	225.04	837.72	2730.59
	IST	1.39	2.81	3.97	6.33	9.74
	MUSIC	0.41	0.94	2.04	4.43	8.48
RA	CS-ADCG	0.77	1.11	1.54	2.00	2.11
	IST	1.48	3.01	6.14	7.29	12.05
	MUSIC	0.46	1.07	2.29	4.62	9.13
Number		11	17	20	25	30
CPA	CS-ADCG	0.50	0.52	0.51	0.63	0.69
	ANM	204.28	2567.29	9735.35	>10 h	>40 h
	IST	1.29	1.39	1.45	1.74	1.87
	MUSIC	0.41	0.43	0.45	0.57	0.62

5. Real Data Experiments

In this section, we validate the effectiveness of CS-ADCG in DOA estimation of automotive MMW radar through a set of real data. The automotive MMW radar which operates frequency at 77GHz and can virtually create 32 channels is provided by Beijing Autoroad Technology Co., Ltd. We installed two corner reflectors at the same height position, with a distance of 70 cm between the two corner reflector centers. We installed the radar at the same height as the corner reflectors. The distance between the radar and the corner reflectors is 13.4 m, 20.1 m and 40.1 m, respectively, in order to achieve angle intervals of 3°, 2° and 1° between two corner reflectors. Figure 8 shows the reconstruction results of CS-ADCG, ANM, IST and MUSIC algorithms for datasets with angular separations of 3°, 2° and 1° at three different snapshots, respectively. Figure 8a–c show reconstructions where the angular between the two corner reflectors is 3°. Figure 8d–f show reconstructions where the angular between the two corner reflectors is 2°. Figure 8g–i show reconstructions where the angular between the two corner reflectors is 1°. Table 2 presents the numerical results of each experiment in Figure 8. The values represent the angle between two peaks in the reconstruction results. For the IST and MUSIC algorithms, we select two main peaks to calculate the angular interval between two corner reflectors.

From Figure 8a–c, it can be seen that all four algorithms are effective in reconstructing two signal sources when the angle between the two corner reflectors is 3°. It cannot be ignored that the reconstruction results of the IST algorithm contain many additional outliers.

We have increased the distance between the corner reflectors and the radar so that the angle between the corner reflectors is 2°. From Figure 8d–f, it can be seen that the CS-ADCG algorithm effectively reconstructs two sources. There are still additional outliers in the reconstruction results of the IST algorithm. It should also be pointed out that the MUSIC algorithm significantly reduces the scattering coefficient of the second corner reflector, leading to a potential oversight of the second corner reflector in the identification of road targets. The same issue is observed with the IST algorithm in Figure 8f.

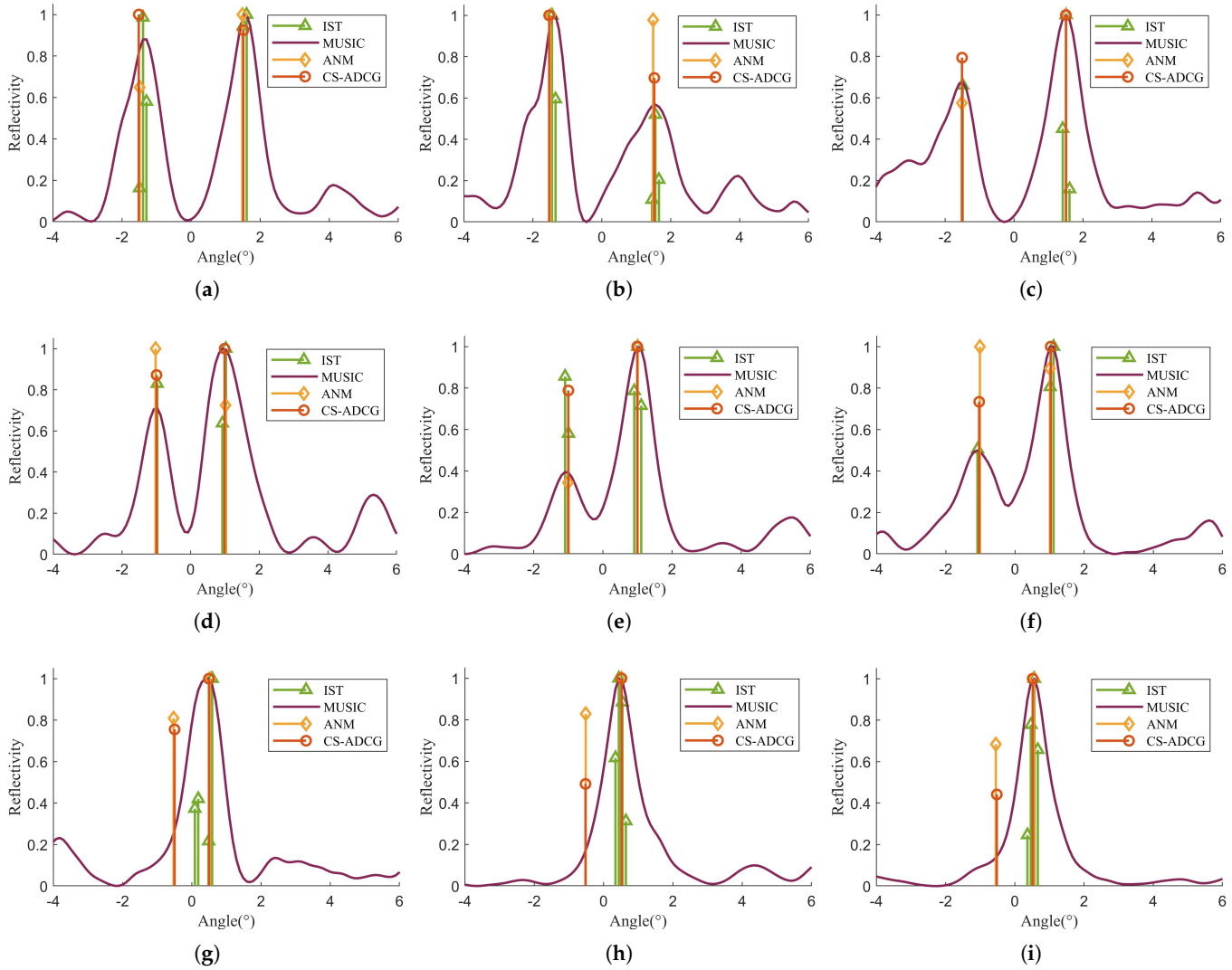


Figure 8. The reconstruction result of two corner reflectors. (**a**–**c**) The angle interval between the corner reflectors is 3°. (**d**–**f**) The angle interval between the corner reflectors is 2°. (**g**–**i**) The angle interval between the corner reflectors is 1°.

Table 2. Numerical results of the CS-ADCG, ANM, IST and MUSIC algorithms for two corner reflectors with angle intervals of 3°, 2° and 1°. The values represent the angle between two peaks in the reconstruction results.

	CS-ADCG			**ANM**			**IST**			**MUSIC**		
Angle Interval of 3°	3.03	3.05	3.01	2.98	2.98	3.02	3.00	3.00	3.00	2.90	2.90	3.00
Angle Interval of 2°	1.98	1.99	1.98	2.03	2.04	2.03	2.00	2.10	2.00	1.90	2.10	1.90
Angle Interval of 1°	0.99	1.03	1.04	1.05	1.03	1.09	\	\	\	\	\	\

In Figure 8g–i, where the angle between the corner reflectors is merely 1°, both IST and MUSIC algorithms fail to effectively discern two corner reflectors. The CS-ADCG and ANM algorithms still successfully reconstruct corner reflectors with an approximate separation of 1°, demonstrating its effectiveness and resolution performance over IST and MUSIC algorithms in real data experiments. The values in Table 2 also confirm this conclusion. Another point to mention is that, unlike the IST algorithm, the reconstruction results of

the CS-ADCG algorithm are not confined to artificially divided grids, indicating that its reconstructions are not affected by the off-grid effect.

6. Conclusions

High-accuracy and high-resolution DOA estimation has always been one of the most critical issues for automotive MMW radar systems. Although traditional CS methods can overcome the limitations of Rayleigh resolution, their accuracy and resolution are limited by the off-grid effect. In this paper, we propose a gridless algorithm for DOA estimation of the automotive MMW radar system and name it the CS-ADCG algorithm. The proposed algorithm takes the ADCG algorithm as the kernel and references traditional CS methods, effectively solving the off-grid effect. Simulation experiments have shown that our proposed gridless algorithm has higher accuracy and resolution compared to IST and MUSIC algorithms and higher efficiency than ANM. We also validated the effectiveness of the CS-ADCG algorithm through real data experiments. Experiments with real data also confirm that the CS-ADCG algorithm is not limited by the off-grid effect and possesses better performance than IST and MUSIC algorithms. Moving forward, we plan to conduct research aimed at enhancing the efficiency of the CS-ADCG algorithm.

Author Contributions: Methodology & writing—review, M.S.; Data curation, Y.Z. and J.Z.; Editing, Y.F.; Project administration, Z.Z. and B.Z. All authors have read and agreed to the published version of the manuscript.

Funding: This research received no external funding.

Data Availability Statement: The original contributions presented in this study are included in the article. Further inquiries can be directed to the corresponding author.

Conflicts of Interest: Author Jie Zhao was employed by the company Beijing Autoroad Technology Co., Ltd. The remaining authors declare that the research was conducted in the absence of any commercial or financial relationships that could be construed as a potential conflict of interest.

References

1. Levy-Israel, M.; Bilik, I.; Tabrikian, J. MCRB on DOA estimation for automotive MIMO radar in the presence of multipath. *IEEE Trans. Aerosp. Electron. Syst.* **2023**, *59*, 4831–4843. [CrossRef]
2. Baral, A.B.; Torlak, M. Joint Doppler frequency and direction of arrival estimation for TDM MIMO automotive radars. *IEEE J. Sel. Top. Signal Process.* **2021**, *15*, 980–995. [CrossRef]
3. Zhang, H.; Liu, W.; Zhang, Q.; Liu, B. Joint Customer Assignment, Power Allocation, and Subchannel Allocation in a UAV-Based Joint Radar and Communication Network. *IEEE Internet Things J.* **2024**, *11*, 29643–29660. [CrossRef]
4. Zhang, H.; Weijian, L.; Zhang, Q.; Taiyong, F. A robust joint frequency spectrum and power allocation strategy in a coexisting radar and communication system. *Chin. J. Aeronaut.* **2024**, *37*, 393–409. [CrossRef]
5. Sun, S.; Petropulu, A.P.; Poor, H.V. MIMO radar for advanced driver-assistance systems and autonomous driving: Advantages and challenges. *IEEE Signal Process. Mag.* **2020**, *37*, 98–117. [CrossRef]
6. Wang, X.; Zhai, W.; Zhang, X.; Wang, X.; Amin, M.G. Enhanced Automotive Sensing Assisted by Joint Communication and Cognitive Sparse MIMO Radar. *IEEE Trans. Aerosp. Electron. Syst.* **2023**, *59*, 4782–4799. [CrossRef]
7. Sun, S.; Zhang, Y.D. 4D automotive radar sensing for autonomous vehicles: A sparsity-oriented approach. *IEEE J. Sel. Top. Signal Process.* **2021**, *15*, 879–891. [CrossRef]
8. Engels, F.; Heidenreich, P.; Wintermantel, M.; Stäcker, L.; Al Kadi, M.; Zoubir, A.M. Automotive radar signal processing: Research directions and practical challenges. *IEEE J. Sel. Top. Signal Process.* **2021**, *15*, 865–878. [CrossRef]
9. Schmidt, R. Multiple emitter location and signal parameter estimation. *IEEE Trans. Antennas Propag.* **1986**, *34*, 276–280. [CrossRef]
10. Liu, Z.; Wu, J.; Yang, S.; Lu, W. DOA estimation method based on EMD and MUSIC for mutual interference in FMCW automotive radars. *IEEE Geosci. Remote Sens. Lett.* **2021**, *19*, 1–5. [CrossRef]
11. Ding, X.; Xu, W.; Wang, Y.; Li, Y.; Huang, Y. Wideband 2D DoA Estimation with Uniform Circular Array. *IEEE Sens. J.* **2024**, *24*, 11585–11598. [CrossRef]
12. Roy, R.; Kailath, T. ESPRIT-estimation of signal parameters via rotational invariance techniques. *IEEE Trans. Acoust. Speech Signal Process.* **1989**, *37*, 984–995. [CrossRef]

13. Kim, S.; Oh, D.; Lee, J. Joint DFT-ESPRIT estimation for TOA and DOA in vehicle FMCW radars. *IEEE Antennas Wirel. Propag. Lett.* **2015**, *14*, 1710–1713. [CrossRef]
14. Candes, E.J.; Romberg, J.; Tao, T. Robust uncertainty principles: Exact signal reconstruction from highly incomplete frequency information. *IEEE Trans. Inf. Theory* **2006**, *52*, 489–509. [CrossRef]
15. Candes, E.J.; Tao, T. The Dantzig selector: Statistical estimation when p is much larger than n. *Ann. Statist.* **2007**, *35*, 2313–2351.
16. Yuan, X.; Brady, D.J.; Katsaggelos, A.K. Snapshot compressive imaging: Theory, algorithms, and applications. *IEEE Signal Process. Mag.* **2021**, *38*, 65–88. [CrossRef]
17. Tan, Z.; Eldar, Y.C.; Nehorai, A. Direction of arrival estimation using co-prime arrays: A super resolution viewpoint. *IEEE Trans. Signal Process.* **2014**, *62*, 5565–5576. [CrossRef]
18. Li, W.T.; Lei, Y.J.; Shi, X.W. DOA estimation of time-modulated linear array based on sparse signal recovery. *IEEE Antennas Wirel. Propag. Lett.* **2017**, *16*, 2336–2340. [CrossRef]
19. Leite, W.S.; de Lamare, R.C. List-based OMP and an enhanced model for DOA estimation with nonuniform arrays. *IEEE Trans. Aerosp. Electron. Syst.* **2021**, *57*, 4457–4464. [CrossRef]
20. Delgado, A.V.; Sánchez-Fernández, M.; Venturino, L.; Tulino, A. Super-resolution in automotive pulse radars. *IEEE J. Sel. Top. Signal Process.* **2021**, *15*, 913–926. [CrossRef]
21. Amani, N.; Jansen, F.; Filippi, A.; Ivashina, M.V.; Maaskant, R. Sparse automotive MIMO radar for super-resolution single snapshot DOA estimation with mutual coupling. *IEEE Access* **2021**, *9*, 146822–146829. [CrossRef]
22. Zhang, H.; Wei, S.; Cai, X.; Nie, L.; Wang, M.; Shi, J.; Cui, G. Dual-domain Feature-oriented Interference Suppression for FMCW Automotive Radar. *IEEE Sens. J.* **2024**, *24*, 6405–6417. [CrossRef]
23. Chi, Y.; Scharf, L.L.; Pezeshki, A.; Calderbank, A.R. Sensitivity to basis mismatch in compressed sensing. *IEEE Trans. Signal Process.* **2011**, *59*, 2182–2195. [CrossRef]
24. Herman, M.A.; Strohmer, T. General deviants: An analysis of perturbations in compressed sensing. *IEEE J. Sel. Top. Signal Process.* **2010**, *4*, 342–349. [CrossRef]
25. Yang, Z.; Xie, L.; Zhang, C. Off-grid direction of arrival estimation using sparse Bayesian inference. *IEEE Trans. Signal Process.* **2012**, *61*, 38–43. [CrossRef]
26. Candes, E.J.; Romberg, J.K.; Tao, T. Stable signal recovery from incomplete and inaccurate measurements. *Commun. Pure Appl. Math. J. Issued Courant Inst. Math. Sci.* **2006**, *59*, 1207–1223. [CrossRef]
27. Yang, J.; Yang, Y. Sparse Bayesian DOA estimation using hierarchical synthesis lasso priors for off-grid signals. *IEEE Trans. Signal Process.* **2020**, *68*, 872–884. [CrossRef]
28. Yang, Z.; Xie, L. Enhancing sparsity and resolution via reweighted atomic norm minimization. *IEEE Trans. Signal Process.* **2015**, *64*, 995–1006. [CrossRef]
29. Chu, Y.; Wei, Z.; Yang, Z. New reweighted atomic norm minimization approach for line spectral estimation. *Signal Process.* **2023**, *206*, 108897. [CrossRef]
30. Tang, G.; Bhaskar, B.N.; Shah, P.; Recht, B. Compressed sensing off the grid. *IEEE Trans. Inf. Theory* **2013**, *59*, 7465–7490. [CrossRef]
31. Yang, Z.; Li, J.; Stoica, P.; Xie, L. Sparse methods for direction-of-arrival estimation. In *Academic Press Library in Signal Processing, Volume 7*; Elsevier: Amsterdam, The Netherlands, 2018; pp. 509–581.
32. Zhang, Z.; Wang, Y.; Tian, Z. Efficient two-dimensional line spectrum estimation based on decoupled atomic norm minimization. *Signal Process.* **2019**, *163*, 95–106. [CrossRef]
33. Tang, W.G.; Jiang, H.; Zhang, Q. Range-angle decoupling and estimation for FDA-MIMO radar via atomic norm minimization and accelerated proximal gradient. *IEEE Signal Process. Lett.* **2020**, *27*, 366–370. [CrossRef]
34. Lau, K.H.; Ng, C.K.; Song, J. Low-Complex Single-Snapshot DoA-Estimation With Higher Degree of Atomic Separation-Freedom in a MU-MIMO System Aided by Prior Information. *IEEE Signal Process. Lett.* **2023**, *30*, 349–353. [CrossRef]
35. Zhang, X.; Zheng, Z.; Wang, W.Q.; So, H.C. DOA estimation of coherent sources using coprime array via atomic norm minimization. *IEEE Signal Process. Lett.* **2022**, *29*, 1312–1316. [CrossRef]
36. Chu, Y.; Wei, Z.; Yang, Z.; Ng, D.W.K. Channel Estimation for RIS-Aided MIMO Systems: A Partially Decoupled Atomic Norm Minimization Approach. *IEEE Trans. Wirel. Commun.* **2024**, *23*, 16048–16061. [CrossRef]
37. Li, J.; Li, Y.; Zhang, X. Two-dimensional off-grid DOA estimation using unfolded parallel coprime array. *IEEE Commun. Lett.* **2018**, *22*, 2495–2498. [CrossRef]
38. Shen, F.F.; Liu, Y.M.; Zhao, G.H.; Chen, X.Y.; Li, X.P. Sparsity-based off-grid DOA estimation with uniform rectangular arrays. *IEEE Sens. J.* **2018**, *18*, 3384–3390. [CrossRef]
39. Badiu, M.A.; Hansen, T.L.; Fleury, B.H. Variational Bayesian inference of line spectra. *IEEE Trans. Signal Process.* **2017**, *65*, 2247–2261. [CrossRef]
40. Yang, Z.; Xie, L.; Zhang, C. A discretization-free sparse and parametric approach for linear array signal processing. *IEEE Trans. Signal Process.* **2014**, *62*, 4959–4973. [CrossRef]

41. Wu, X.; Zhu, W.P.; Yan, J. A fast gridless covariance matrix reconstruction method for one-and two-dimensional direction-of-arrival estimation. *IEEE Sens. J.* **2017**, *17*, 4916–4927. [CrossRef]
42. Wagner, M.; Park, Y.; Gerstoft, P. Gridless DOA estimation and root-MUSIC for non-uniform linear arrays. *IEEE Trans. Signal Process.* **2021**, *69*, 2144–2157. [CrossRef]
43. Boyd, N.; Schiebinger, G.; Recht, B. The alternating descent conditional gradient method for sparse inverse problems. *SIAM J. Optim.* **2017**, *27*, 616–639. [CrossRef]
44. Kakkavas, A.; Wymeersch, H.; Seco-Granados, G.; García, M.H.C.; Stirling-Gallacher, R.A.; Nossek, J.A. Power allocation and parameter estimation for multipath-based 5G positioning. *IEEE Trans. Wirel. Commun.* **2021**, *20*, 7302–7316. [CrossRef]
45. Huang, J.; Sun, M.; Ma, J.; Chi, Y. Super-resolution image reconstruction for high-density three-dimensional single-molecule microscopy. *IEEE Trans. Comput. Imaging* **2017**, *3*, 763–773. [CrossRef]
46. Daubechies, I.; Defrise, M.; De Mol, C. An iterative thresholding algorithm for linear inverse problems with a sparsity constraint. *Commun. Pure Appl. Math. J. Issued Courant Inst. Math. Sci.* **2004**, *57*, 1413–1457. [CrossRef]
47. Frank, M.; Wolfe, P. An algorithm for quadratic programming. *Nav. Res. Logist. Q.* **1956**, *3*, 95–110. [CrossRef]

Disclaimer/Publisher's Note: The statements, opinions and data contained in all publications are solely those of the individual author(s) and contributor(s) and not of MDPI and/or the editor(s). MDPI and/or the editor(s) disclaim responsibility for any injury to people or property resulting from any ideas, methods, instructions or products referred to in the content.